Tip-induced creation and Jahn-Teller distortions of sulfur vacancies in single-layer MoS$_2$

Daniel Jansen [1], Tfyeche Tounsi [1], Jeison Fischer [1], Arkady V. Krasheninnikov [2], Thomas Michely [1],
Hannu-Pekka Komsa [3], and Wouter Jolie [1]

^{1}*II. Physikalisches Institut, Universität zu Köln, Zülpicher Straße 77, 50937 Köln, Germany*
^{2}*Institute of Ion Beam Physics and Materials Research, Helmholtz-Zentrum Dresden-Rossendorf, 01328 Dresden, Germany*
^{3}*Faculty of Information Technology and Electrical Engineering, University of Oulu, FI-90014 Oulu, Finland*

We present an atomically precise technique to create sulfur vacancies and control their atomic configurations in single-layer MoS$_2$. It involves adsorbed Fe atoms and the tip of a scanning tunneling microscope, which enables single sulfur removal from the top sulfur layer at the initial position of Fe. Using scanning tunneling spectroscopy, we show that the STM tip can also induce two Jahn-Teller distorted states with reduced orbital symmetry in the sulfur vacancies. Density functional theory calculations rationalize our experimental results. Additionally, we provide evidence for molecule-like hybrid orbitals in artificially created sulfur vacancy dimers, which illustrates the potential of our technique for the development of extended defect lattices and tailored electronic band structures.

Point defects in semiconducting two-dimensional (2D) transition metal dichalcogenides (TMDs) yield atomically precise quantum states of matter. Defects can induce isolated in-gap states [1–3], which are envisioned to have potential as qubits [4,5] or single-photon emitters [4,6]. Having access to such isolated levels enables detection of physical properties related to nanomagnetism [7–9], spin-orbit coupling [10], or chemical bond formation [10–12].

One way to create an isolated defect is via atom removal. Vacancies can be introduced in TMDs through impacts of energetic electrons in transmission electron microscopy [13–15], ion irradiation [16–19], as well as via annealing in ultrahigh vacuum (UHV) [1]. While the concentration of vacancies can be controlled to some extent via ion/electron irradiation fluence and particle energy, annealing time and sample temperature, these techniques tend to create other types of defects as well, often with unknown atomic structure. The elevated temperatures can also lead to diffusion and agglomeration of vacancies [20]. Hence, a method able to locally create and probe a single type of vacancy in 2D TMDs remains elusive. It would allow unambiguous identification of theoretical predictions, such as a Jahn-Teller distortion when an extra electron occupies one of the in-gap states [6,21,22].

In this paper, we employ an atomic manipulation approach to create single vacancies in the top sulfur layer of single-layer MoS$_2$. We use Fe atoms adsorbed on MoS$_2$ as atomic-scale markers for vacancy creation. A detailed characterization of isolated vacancies reveals two Jahn-Teller distorted states when the vacancy is charged. Creating a vacancy dimer shows the formation of hybridized states, while no additional distortion is observed upon charging.

All scanning tunneling microscopy (STM) and spectroscopy (STS) measurements were performed in a UHV low-temperature STM setup with an operating temperature of 6 K. MoS$_2$ grown on Gr on Ir(111) is quasi-freestanding, as evidenced by its large band gap [23], sharp valence band [24],

and narrow photoluminescence peak [24]. The Ir(111) crystal was first cleaned by cycles of 1.5 keV Ar$^+$ ion beam exposure and annealed to 1550 K. Subsequently, single crystal Gr was grown using the growth method described in Ref. [25]. MoS$_2$ islands were grown according to Ref. [26] using an e-beam evaporator for Mo and a Knudsen cell for sulfur supply. The MoS$_2$ islands were grown at room temperature with a Mo flux of $1.14 \times 10^{16} \frac{\text{atoms}}{\text{m}^2 \cdot \text{s}}$, a deposition time of 600 s and a sulfur pressure of 6×10^{-9} mbar. Afterwards the sample was annealed in a sulfur pressure of 3×10^{-9} mbar at 1050 K for 300 s, resulting in virtually defect-free single-layer MoS$_2$ islands with small second layer islands on top. Single Fe atom evaporation was performed using an e-beam evaporator at a sample temperature of 8 K. An STM image of the as-grown sample is presented in Fig. 1(a). It becomes apparent, that Fe on MoS$_2$ is nonmobile and does not cluster at low Fe densities.

Sulfur vacancies can be created with high reproducibility by the following procedure: First, the STM tip is positioned over an Fe adatom and approached by decreasing the bias voltage V_{bias} and increasing the tunneling current I_{set} with closed feedback loop. The tip-adatom separation is reduced until a sudden change in the measured tip height is detected. Typical values are $V_{bias} \approx 30$ mV and $I_{set} \approx 1$ nA. After this event, the tip height is increased to scanning parameters (typically $V_{bias} = 1$ V and $I_{set} = 100$ pA). In the large majority of attempts, this procedure creates a sulfur vacancy. A series of STM images showing the subsequent creation of two neighboring sulfur vacancies is presented in Figs. 1(b)–1(d).

A model interpreting the observations is shown in Fig. 1(e). The pick-up event involves the adsorbed Fe atom together with a single sulfur atom, leaving a sulfur vacancy in MoS$_2$ behind. According to our DFT calculations, the Fe-sulfur bond alone is not sufficient to create a vacancy. Additional effects, such as the electric field between tip and surface [27], as well as vibrations induced by tunneling electrons can
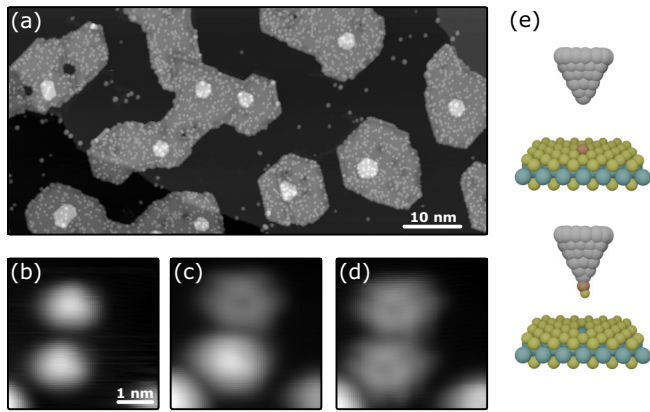
FIG. 1. Local creation of sulfur vacancies. (a) STM image of single-layer and bilayer MoS_2 islands on Gr/Ir(111) covered with Fe adatoms ($V_{bias} = 1$ V, $I_{set} = 100$ pA, image sizes: 200×90 nm^2). [(b)–(d)] Step-by-step creation of sulfur vacancies. (b) Two adjacent Fe adatoms on MoS_2 ($V_{bias} = 1$ V, $I_{set} = 100$ pA, image size: 4×4 nm^2). (c) Upper Fe adatom removed and sulfur vacancy created at its location ($V_{bias} = 500$ mV, $I_{set} = 100$ pA). (d) Second Fe adatom removed and vacancy created ($V_{bias} = 500$ mV, $I_{set} = 100$ pA). (e) Sketch visualizing how the STM tip creates sulfur vacancies in MoS_2.

facilitate pick-up, though a full picture of the mechanism lies beyond the scope of the present study. While the chemical bond between tip and Fe strongly depends on apex geometry and chemical composition, the Fe-sulfur bond is well defined for every pick-up event. This leads to high reproducibility of the vacancy creation process, as long as the bond between Fe and STM tip is strong enough to initiate the pick-up event. This is in contrast to direct sulfur pick-up events without Fe adatoms reported earlier for bulk MoS_2 [28], which we found not to be applicable to single-layer MoS_2 islands.

The electronic characterization of an isolated sulfur vacancy created using our atomic manipulation approach is presented in Fig. 2. An STM image of a single vacancy is shown in Fig. 2(a). Its appearance depends on the applied bias voltage, which is discussed in Fig. S1 in Ref. [29]. An STS point spectrum acquired on pristine MoS_2 [Fig. 2(b)] displays its band gap [23]. Point spectra taken on the defect lobes reveal the existence of three peaks in the band gap of MoS_2, as shown in Fig. 2(c). Corresponding dI/dV maps measured at the respective peak energies above the Fermi level and presented in Fig. 2(d) show two nearly-equivalent orbitals with C_{3v} symmetry, the lowest unoccupied defect orbitals LUDO and LUDO+1. In contrast, the dI/dV map measured close
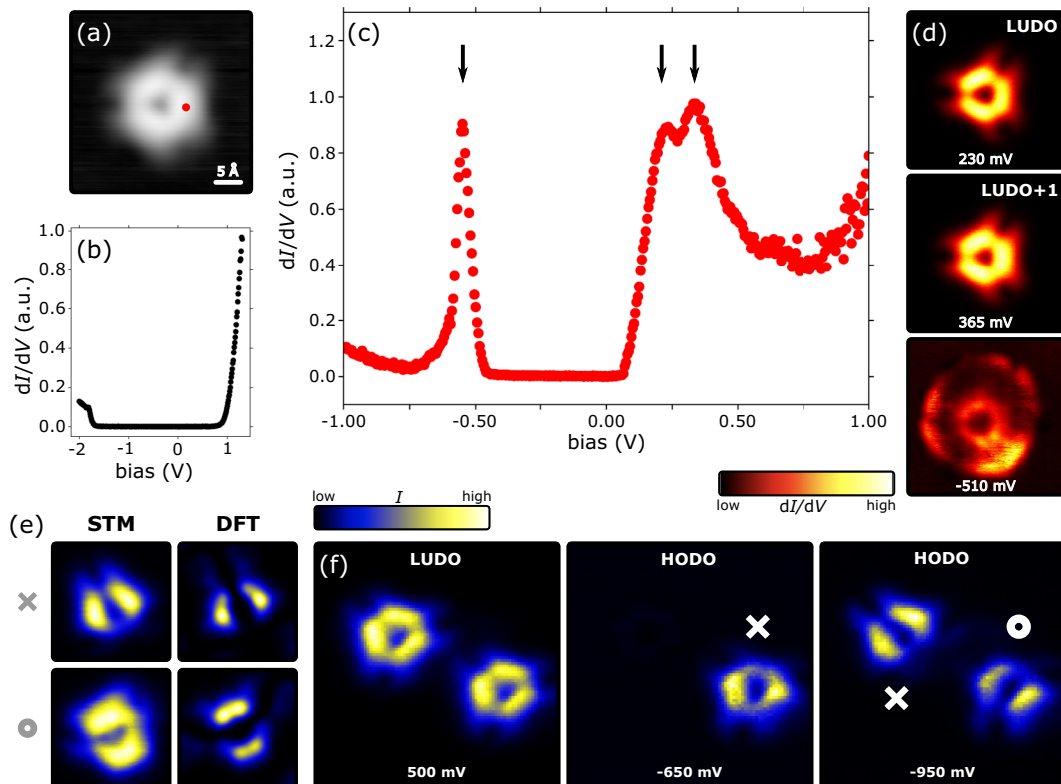

FIG. 2. Spectroscopic investigation of sulfur vacancies. (a) STM image of a created sulfur vacancy ($V_{bias} = 1$ V, $I_{set} = 100$ pA, image size: 3×3 nm^2). The red spot marks the location where the spectrum presented in (c) was measured. (b) dI/dV spectrum ($V_{stab} = 1.3$ V, $I_{stab} = 100$ pA, $V_{mod} = 10$ mV) measured on pristine MoS_2. (c) dI/dV spectrum ($V_{stab} = 1$ V, $I_{stab} = 500$ pA, $V_{mod} = 2$ mV) measured on the vacancy, revealing three peaks in the band gap of MoS_2. (d) Constant-height dI/dV maps (size: 3×3 nm^2) measured at energies indicated by black arrows in (c). (e) Constant-height current maps of the two distinct symmetry-broken HODO orbitals and corresponding DFT simulations. The two types of orbitals are denoted by crosses ($\times$) and circles ($\bigcirc$). (f) Series of current maps showing transitions between the two symmetry-broken states (image sizes: 7×7 nm^2).

to the peak energy below the Fermi level reveals a modified orbital shape, surrounded by a pronounced ring.

The origin of the peak in the occupied states and the ring in the dI/dV map is a charging event induced by the STM tip [30]. Applying a bias voltage between tip and sample implies an electric field between them and thus causes the in-gap states of the sulfur vacancy to shift in energy. For large enough negative bias voltages, the LUDO level is pulled below the Fermi energy and occupied by an electron, thus becoming the highest occupied defect orbital (HODO) of the charged vacancy. The peak in the point spectrum of Fig. 2(c) and the ring in the dI/dV map in Fig. 2(d) at -510 mV thus reflect a sudden change in the occupied defect states due to charging and subsequent distribution of that charge. Similar results have previously been obtained for sulfur vacancies in single-layer WS_2 [1].

The absence of additional states in the MoS_2 band gap enables us to access the HODO orbital at high bias voltages at which the vacancy is stably charged, by measuring the tunneling current in constant-height mode. This signal integrates over all states between the Fermi energy and the bias voltage, which in our system is dominated by the HODO only, see Fig. S2 in Ref. [29] for detailed reasoning why constant-height current maps are used to image the HODO. Constant-height maps recording the tunneling current of two representative vacancies are presented in Fig. 2(e). The high-resolution maps reveal two different types of HODOs, denoted as ($\times$) and ($\bigcirc$). Both show a clear symmetry reduction from C_{3v} to C_S. A statistical analysis of 16 vacancies reveals that 10 of the HODOs have the appearance ($\times$), while the remaining 6 display the ($\bigcirc$) orbital shape. These orbitals can transform from one to another when neighboring vacancies are charged. This is demonstrated in Fig. 2(f) for two neighboring vacancies. Their LUDOs are measured at 500 mV. At -650 mV, only one of the vacancies is charged, due to differences in the in-gap state energies of the neutral vacancies, displayed in Fig. S3 in Ref. [29] (see also Ref. [31] therein). Hence, only one HODO is observed, in state ($\times$). Increasing the bias voltage eventually charges the second vacancy. While the latter is in state ($\times$), the other transformed into state ($\bigcirc$).

The behavior of the vacancies upon charging can be understood with the help of density functional theory (DFT). For details on the computational methods we refer to Ref. [29] (see also Refs. [32–38] therein). Negatively charged sulfur vacancies in MoS_2 have been predicted to undergo a JT effect, which distorts the host lattice and spontaneously breaks the (orbital) symmetry from C_{3v} to C_S [6,21,22]. To understand the JT effect in MoS_2 sulfur vacancies, we simulate the energy levels of a MoS_2 vacancy, see Fig. 3(a). The three dangling bonds from Mo atoms (ϕ_a, ϕ_b, and ϕ_c) in C_{3v} symmetry lead to the following symmetry-adapted linear combinations (SALCs): $\phi_1 = \phi_a + \phi_b + \phi_c$, $\phi_2 = 2\phi_a - \phi_b - \phi_c$, and $\phi_3 = \phi_b - \phi_c$, where ϕ_1 belongs to a_1 and ϕ_2 and ϕ_3 to e. The lowest a_1 state is occupied by two electrons and lies close to the VBM [not shown in Fig. 3(a)]. The a_1 state is thus too far away from the Fermi level to be depopulated by the electric field of the tip. The two degenerate e states are unoccupied and fall in the band gap of MoS_2 [39], see Fig. 3(a) (V_S^0 without SOC). The SALCs can be clearly seen in the charge density plots presented in Fig. S4 [29]. Adding SOC partially lifts the
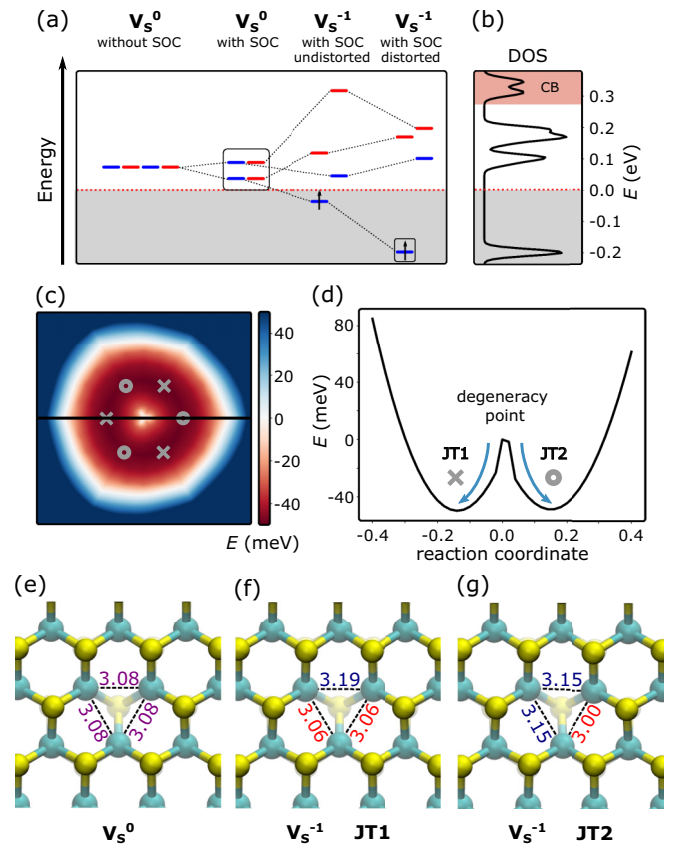

FIG. 3. Jahn-Teller distortions in negatively charged sulfur vacancies. (a) Evolution of sulfur vacancy levels (blue: spin-up, red: spin-down) upon introduction of spin-orbit coupling, charge and lattice distortions. The gray shaded area indicates state occupation and the red dashed line the Fermi level. Black solid boxes emphasize which states are accessible in experiment. (b) DFT calculated DOS of the distorted negatively charged sulfur vacancy. (c) Potential energy surface of the negatively charged sulfur vacancy. Upon charging, the vacancy can relax into two different JT distorted states indicated by crosses ($\times$) and circles ($\bigcirc$), respectively. (d) Slice through the potential energy surface along black line displayed in (c). [(e)–(g)] Structure models of the MoS_2 lattice around the sulfur vacancy for the neutral (e) and charged case in JT1 (f) and JT2 (g) states. The numbers on the dashed lines give the Mo atom separations (angstroms).

degeneracy of the e states, leading to two doubly-degenerate levels [Fig. 3(a) (V_S^0 with SOC)] [40]. These levels correspond to the LUDO and LUDO+1 orbitals found in experiment. Adding an electron to the lowest level lifts all remaining degeneracies, leaving one uncompensated spin below the Fermi energy [Fig. 3(a) (V_S^{-1} with SOC undistorted)]. Relaxing the structure spontaneously distorts the atomic configuration around the vacancy, leading to the energy level configuration of the JT effect in negatively charged MoS_2 sulfur vacancies, presented in Fig. 3(a) (V_S^{-1} with SOC distorted). The corresponding density of states (DOS) is presented in Fig. 3(b). Note that only the HODO is experimentally accessible [solid black box in the level scheme in Fig. 3(a)], since we need to apply a negative bias voltage to charge the vacancy.

Until now theoretical investigations only predicted the existence of one type of JT effect for negatively charged sulfur vacancies in MoS_2 [6,21,22]. Similarly, two recent experimental works on charged sulfur vacancies in single-layer MoS_2 on Gr proposed only one type of distortion to explain the observed orbital symmetry reduction [41,42]. Our investigations, however, reveal that there are two distinct types of JT distortions, denoted JT1 and JT2. They correspond to two imaginary phonon modes and thus two types of lattice distortions. Both are local minima in the potential energy surface (PES) of the system, which is shown in Fig. 3(c). A direct comparison between our experimental maps and DFT simulations of the HODO, shown in Fig. 2(e), makes plain that the two orbitals denoted by ($\times$) and ($\bigcirc$) correspond to JT1 and JT2. We thus indicate the local minima of the PES that correspond to JT1 and JT2 by crosses ($\times$) and circles ($\bigcirc$), respectively. A cut through the PES along the horizontal line indicated in black, is shown in Fig. 3(d). The JT distortion leads to an energy gain of approximately 50 meV compared to the unrelaxed structure, while JT1 and JT2 distortions have the same energy within the accuracy of our DFT calculation. Upon charging, the sulfur vacancy thus spontaneously transitions into one of the JT distorted states with similar probabilities (blue arrows). The corresponding structural distortions compared to the neutral vacancy configuration [Fig. 3(e)] are shown in Fig. 3(f) and 3(g). A detailed summary of all simulated JT1 and JT2 orbitals is presented in Fig. S5 and S6 [29].

Coming back to the transformation from JT1 to JT2 shown in Fig. 2(f), we can now infer that it is likely caused by the strain field created when a neighboring vacancy becomes JT distorted. Indeed, DFT is able to reproduce the transformation using a directional strain field, see Fig. S7 [29]. Apparently the elastic energy is minimized, when the two neighboring vacancies are in different JT states.

To demonstrate the potential of our vacancy creation technique for the study of larger tailor-made sulfur vacancy structures, we created and characterized a vacancy dimer, see Fig. 4(a). The vacancies are created in next-nearest neighbor distance $d = \sqrt{3}a$, with a being the MoS_2 lattice constant. As can be seen in Fig. 4(b) (left column) the dI/dV intensity distribution of the hybrid orbitals are distinct from the LUDO and LUDO+1 of isolated vacancies. The observed behavior is reminiscent of bonding and antibonding molecular orbitals, which is reproduced in the corresponding DFT maps (right column). While the measured dI/dV signal seems to suggest that the antibonding state is lower in energy, as also observed for coupled quantum corrals confining holelike quasiparticles [43], an inspection of the total DOS does not allow for such an unambiguous identification, see Fig. S8 [29]. Nevertheless, these hybridized orbitals form two unoccupied bands in a one-dimensional vacancy chain, according to our DFT calculations presented in Fig. 4(c). Such an assembly of large vacancy defect structures can be realized with our atomically precise vacancy creation method, if the adatoms used as markers can be manipulated laterally with sufficiently high fidelity prior to pick-up. The chains would have great potential for 2D devices made from semiconducting TMDs, in which transport properties are often governed by defect states [44,45]. While for Fe adatoms on MoS_2 the manipulation efficiency is
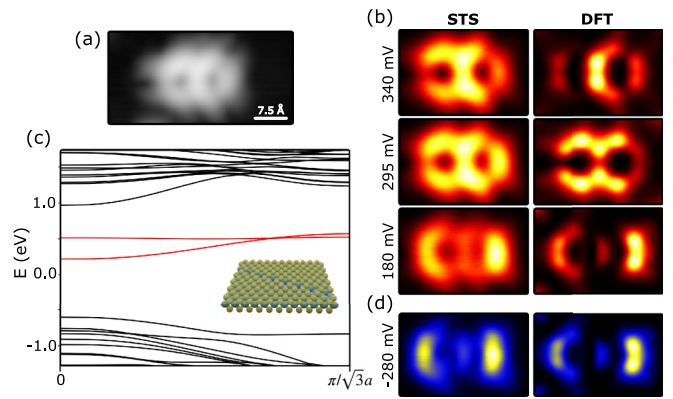

FIG. 4. Artificial sulfur vacancy structures in MoS_2. (a) STM image of a sulfur vacancy dimer ($V_{bias} = 1$ V, $I_{set} = 100$ pA, image size: 4×2 nm^2). (b) Constant-height dI/dV maps measured at the indicated V_{bias} compared to DFT simulated DOS maps of the corresponding hybrid orbitals (image sizes: 2.2×1.4 nm^2). (c) Band structure of a vacancy chain (model in inset). (d) Constant-height current map of the vacancy dimer in the charged state ($V_{bias} = -280$ mV).

limited, it is plausible that several adatom species exist, which can be laterally manipulated, while simultaneously forming sufficiently strong bonds with the chalcogen atoms to enable pick-up.

Applying a negative bias voltage enables us to charge the dimer. Its HODO is shown in Fig. 4(d), in good agreement with the corresponding DFT simulation for single electron charging. DFT simulations for all orbitals of the singly and doubly charged vacancy dimer are provided in Fig. S9 [29]. The LUDO of the neutral dimer (measured at 180 mV) and the HODO of the charged dimer (measured at -280 mV) have the same shape and hence display no JT distortion, in stark contrast to the spontaneous symmetry breaking observed in the charged single vacancy. This can be rationalized by the fact that the dimer geometry reduces the symmetry and consequently lifts the orbital degeneracy. It emphasizes the importance of the environment of single vacancies, to enable detection of their pristine properties.

In summary, we have developed a technique for atomically precise creation of point defects in 2D TMDs, involving adsorbed atoms and the tip of an STM. Sulfur vacancies in the top sulfur layer of single-layer MoS_2 are created by picking up single Fe adatoms from the surface. Tip-induced gating was used to manipulate sulfur vacancies into a negatively charged state, revealing the existence of two types of JT distortions, which can be transformed into one another by their mutual interaction. Furthermore, we studied the orbital overlap of sulfur vacancy states using the described creation approach and revealed strong hybridization.

[1] B. Schuler, D. Y. Qiu, S. Refaely-Abramson, C. Kastl, C. T. Chen, S. Barja, R. J. Koch, D. F. Ogletree, S. Aloni, A. M. Schwartzberg, J. B. Neaton, S. G. Louie, and A. Weber-Bargioni, Large spin-orbit splitting of deep in-gap defect states of engineered sulfur vacancies in monolayer WS_2, Phys. Rev. Lett. **123**, 076801 (2019).

[2] G.-J. Zhu, Y.-G. Xu, X.-G. Gong, J.-H. Yang, and B. I. Yakobson, Dimensionality-inhibited chemical doping in two-dimensional semiconductors: The phosphorene and MoS_2 from charge-correction method, Nano Lett. **21**, 6711 (2021).

[3] D. J. Trainer, J. Nieminen, F. Bobba, B. Wang, X. Xi, A. Bansil, and M. Iavarone, Visualization of defect induced in-gap states in monolayer MoS_2, npj 2D Mater. Appl. **6**, 13 (2022).

[4] G. Zhang, Y. Cheng, J.-P. Chou, and A. Gali, Material platforms for defect qubits and single-photon emitters, Appl. Phys. Rev. **7**, 031308 (2020).

[5] S. Li, G. Thiering, P. Udvarhelyi, V. Ivády, and A. Gali, Carbon defect qubit in two-dimensional WS_2, Nat. Commun. **13**, 1210 (2022).

[6] S. Gupta, J.-H. Yang, and B. I. Yakobson, Two-level quantum systems in two-dimensional materials for single photon emission, Nano Lett. **19**, 408 (2019).

[7] C. Zhang, C. Wang, F. Yang, J.-K. Huang, L.-J. Li, W. Yao, W. Ji, and C.-K. Shih, Engineering point-defect states in monolayer WSe_2, ACS Nano **13**, 1595 (2019).

[8] K. A. Cochrane, J.-H. Lee, C. Kastl, J. B. Haber, T. Zhang, A. Kozhakhmetov, J. A. Robinson, M. Terrones, J. Repp, J. B. Neaton, A. Weber-Bargioni, and B. Schuler, Spin-dependent vibronic response of a carbon radical ion in two-dimensional WS_2, Nat. Commun. **12**, 7287 (2021).

[9] S. Trishin, C. Lotze, N. Krane, and K. J. Franke, Electronic and magnetic properties of single chalcogen vacancies in MoS_2/Au(111), Phys. Rev. B **108**, 165414 (2023).

[10] B. Schuler, J.-H. Lee, C. Kastl, K. A. Cochrane, C. T. Chen, S. Refaely-Abramson, S. Yuan, E. van Veen, R. Roldán, N. J. Borys, R. J. Koch, S. Aloni, A. M. Schwartzberg, D. F. Ogletree, J. B. Neaton, and A. Weber-Bargioni, How substitutional point defects in two-dimensional WS_2 induce charge localization, spin-orbit splitting, and strain, ACS Nano **13**, 10520 (2019).

[11] P. Vancsó, G. Z. Magda, J. Pető, J.-Y. Noh, Y.-S. Kim, C. Hwang, L. P. Biró, and L. Tapasztó, The intrinsic defect structure of exfoliated MoS_2 single layers revealed by scanning tunneling microscopy, Sci. Rep. **6**, 29726 (2016).

[12] Y. Zhao, M. Tripathi, K. Čerņevičs, A. Avsar, H. G. Ji, J. F. Gonzalez Marin, C.-Y. Cheon, Z. Wang, O. V. Yazyev, and A. Kis, Electrical spectroscopy of defect states and their hybridization in monolayer MoS_2, Nat. Commun. **14**, 44 (2023).

[13] W. Zhou, X. Zou, S. Najmaei, Z. Liu, Y. Shi, J. Kong, J. Lou, P. M. Ajayan, B. I. Yakobson, and J.-C. Idrobo, Intrinsic structural defects in monolayer molybdenum disulfide, Nano Lett. **13**, 2615 (2013).

[14] H.-P. Komsa, S. Kurasch, O. Lehtinen, U. Kaiser, and A. V. Krasheninnikov, From point to extended defects in two-dimensional MoS_2: Evolution of atomic structure under electron irradiation, Phys. Rev. B **88**, 035301 (2013).

[15] J. Hong, Z. Hu, M. Probert, K. Li, D. Lv, X. Yang, L. Gu, N. Mao, Q. Feng, L. Xie, W. Zhang, D. Wu, Z. Zhang, C. Jin, W. Ji, X. Zhang, J. Yuan, and Z. Zhang, Exploring atomic defects in molybdenum disulphide monolayers, Nat. Commun. **6**, 6293 (2015).

[16] E. Mitterreiter, B. Schuler, K. A. Cochrane, U. Wurstbauer, A. Weber-Bargioni, C. Kastl, and A. W. Holleitner, Atomistic positioning of defects in helium ion treated single-layer MoS_2, Nano Lett. **20**, 4437 (2020).

[17] P. Valerius, S. Kretschmer, B. V. Senkovskiy, S. Wu, J. Hall, A. Herman, N. Ehlen, M. Ghorbani-Asl, A. Grüneis, A. V. Krasheninnikov, and T. Michely, Reversible crystalline-to-amorphous phase transformation in monolayer MoS_2 under grazing ion irradiation, 2D Mater. **7**, 025005 (2020).

[18] E. Mitterreiter, B. Schuler, A. Micevic, D. Hernangómez-Pérez, K. Barthelmi, K. A. Cochrane, J. Kiemle, F. Sigger, J. Klein, E. Wong, E. S. Bernard, K. Watanabe, T. Taniguchi, M. Lorke, F. Jahnke, J. J. Finley, A. M. Schwartzberg, D. Y. Qiu, S. Rafaely-Abramson, A. W. Holleitner *et al.*, The role of chalcogen vacancies for atomic defect emission in MoS_2, Nat. Commun. **12**, 3822 (2021).

[19] B. Ozden, T. Zhang, M. Liu, A. Fest, D. A. Pearson, E. Khan, S. Uprety, J. E. Razon, J. Cherry, K. Fujisawa, H. Liu, N. Perea-López, K. Wang, T. Isaacs-Smith, M. Park, and M. Terrones, Engineering vacancies for the creation of antisite defects in chemical vapor deposition grown monolayer MoS_2 and WS_2 via proton irradiation, ACS Nano **17**, 25101 (2023).

[20] H. Fang, H. Mahalingam, X. Li, X. Han, Z. Qiu, Y. Han, K. Noori, D. Dulal, H. Chen, P. Lyu, T. Yang, J. Li, C. Su, W. Chen, Y. Cai, A. H. C. Neto, K. S. Novoselov, A. Rodin, and J. Lu, Atomically-precise vacancy-assembled quantum antidots, Nat. Nanotechnol. **18**, 1401 (2023).

[21] H.-P. Komsa and A. V. Krasheninnikov, Native defects in bulk and monolayer MoS_2 from first principles, Phys. Rev. B **91**, 125304 (2015).

[22] A. M. Z. Tan, C. Freysoldt, and R. G. Hennig, Stability of charged sulfur vacancies in 2D and bulk MoS_2 from plane-wave density functional theory with electrostatic corrections, Phys. Rev. Mater. **4**, 064004 (2020).

[23] C. Murray, W. Jolie, J. A. Fischer, J. Hall, C. van Efferen, N. Ehlen, A. Grüneis, C. Busse, and T. Michely, Comprehensive tunneling spectroscopy of quasifreestanding MoS_2 on graphene on Ir(111), Phys. Rev. B **99**, 115434 (2019).

[24] N. Ehlen, J. Hall, B. V. Senkovskiy, M. Hell, J. Li, A. Herman, D. Smirnov, A. Fedorov, V. Y. Voroshnin, G. Di Santo, L. Petaccia, T. Michely, and A. Grüneis, Narrow photoluminescence and Raman peaks of epitaxial MoS_2 on graphene/Ir(111), 2D Mater. **6**, 011006 (2018).

[25] A. T. N'Diaye, J. Coraux, T. N. Plasa, C. Busse, and T. Michely, Structure of epitaxial graphene on Ir(111), New J. Phys. **10**, 043033 (2008).

[26] J. Hall, B. Pielić, C. Murray, W. Jolie, T. Wekking, C. Busse, M. Kralj, and T. Michely, Molecular beam epitaxy of quasi-freestanding transition metal disulphide monolayers on van der Waals substrates: a growth study, 2D Mater. **5**, 025005 (2018).

[27] S. Moradi and A. Sadeghi, Strain-induced high chern number topological insulator state in Fe-or V-decorated MoS_2 monolayers, Phys. Rev. B **109**, 035165 (2024).

[28] S. Hosoki, S. Hosaka, and T. Hasegawa, Surface modification of MoS_2 using an STM, Appl. Surf. Sci. **60-61**, 643 (1992).

[29] See Supplemental Material at http://link.aps.org/supplemental/10.1103/PhysRevB.109.195430 for explanations of appearance of sulfur vacancies in STM images for different bias voltages; details on the use of constant-height current maps to access the HODO orbital; the energetic shift of SOC-split vacancy states; details on computational methods; simulated STM images as well as partial charge density plots of single vacancies; DFT results for the effect of lattice strain on Jahn-Teller distortions; spectroscopic investigation of a vacancy dimer and simulated STM images as well as partial charge density plots of a vacancy dimer.

[30] N. A. Pradhan, N. Liu, C. Silien, and W. Ho, Atomic scale conductance induced by single impurity charging, Phys. Rev. Lett. **94**, 076801 (2005).

[31] C. Murray, C. van Efferen, W. Jolie, J. A. Fischer, J. Hall, A. Rosch, A. V. Krasheninnikov, H.-P. Komsa, and T. Michely, Band bending and valence band quantization at line defects in MoS_2, ACS Nano **14**, 9176 (2020).

[32] G. Kresse and J. Hafner, *Ab initio* molecular dynamics for liquid metals, Phys. Rev. B **47**, 558 (1993).

[33] G. Kresse and J. Furthmüller, Efficiency of *ab-initio* total energy calculations for metals and semiconductors using a plane-wave basis set, Comput. Mater. Sci. **6**, 15 (1996).

[34] G. Kresse and J. Furthmüller, Efficient iterative schemes for *ab initio* total-energy calculations using a plane-wave basis set, Phys. Rev. B **54**, 11169 (1996).

[35] J. P. Perdew, K. Burke, and M. Ernzerhof, Generalized gradient approximation made simple, Phys. Rev. Lett. **77**, 3865 (1996).

[36] S. Grimme, Semiempirical GGA-type density functional constructed with a long-range dispersion correction, J. Comput. Chem. **27**, 1787 (2006).

[37] V. Wang, N. Xu, J.-C. Liu, G. Tang, and W.-T. Geng, VASPKIT: A user-friendly interface facilitating high-throughput computing and analysis using VASP code, Comput. Phys. Commun. **267**, 108033 (2021).

[38] A. Togo and I. Tanaka, First principles phonon calculations in materials science, Scr. Mater. **108**, 1 (2015).

[39] M. Pandey, F. A. Rasmussen, K. Kuhar, T. Olsen, K. W. Jacobsen, and K. S. Thygesen, Defect-tolerant monolayer transition metal dichalcogenides, Nano Lett. **16**, 2234 (2016).

[40] M. A. Khan, M. Erementchouk, J. Hendrickson, and M. N. Leuenberger, Electronic and optical properties of vacancy defects in single-layer transition metal dichalcogenides, Phys. Rev. B **95**, 245435 (2017).

[41] F. Xiang, L. Huberich, P. A. Vargas, R. Torsi, J. Allerbeck, A. M. Z. Tan, C. Dong, P. Ruffieux, R. Fasel, O. Gröning, Y.-C-Lin, R. G. Hennig, J. A. Robinson, and B. Schuler, Charge state-dependent symmetry breaking of atomic defects in transition metal dichalcogenides, Nat. Commun. **15**, 2738 (2024).

[42] T. Aliyar, H. Ma, R. Krishnan, G. Singh, B. Q. Chong, Y. Wang, I. Verzhbitskiy, C. P. Yu Wong, K. E. Johnson Goh, Z. X. Shen, T. S. Koh, R. Rahman, and B. Weber, Symmetry breaking and spin-orbit coupling for individual vacancy-induced in-gap states in MoS_2 monolayers, Nano Lett. **24**, 2142 (2024).

[43] W. Jolie, T.-C. Hung, L. Niggli, B. Verlhac, N. Hauptmann, D. Wegner, and A. A. Khajetoorians, Creating tunable quantum corrals on a Rashba surface alloy, ACS Nano **16**, 4876 (2022).

[44] H. Qiu, T. Xu, Z. Wang, W. Ren, H. Nan, Z. Ni, Q. Chen, S. Yuan, F. Miao, F. Song, G. Long, Y. Shi, L. Sun, J. Wang, and X. Wang, Hopping transport through defect-induced localized states in molybdenum disulphide, Nat. Commun. **4**, 2642 (2013).

[45] S. M. Gali, A. Pershin, A. Lherbier, J.-C. Charlier, and D. Beljonne, Electronic and transport properties in defective MoS_2: impact of sulfur vacancies, J. Phys. Chem. C **124**, 15076 (2020).